Experimental and theoretical study of the photodissociation of bromo-3-fluorobenzene

Daniel Karlsson, O. Anders Borg, Sten Lunell, Jan Davidsson, and Hans O. Karlsson

Citation: The Journal of Chemical Physics **128**, 034307 (2008); doi: 10.1063/1.2819093
View online: http://dx.doi.org/10.1063/1.2819093
View Table of Contents: http://scitation.aip.org/content/aip/journal/jcp/128/3?ver=pdfcov
Published by the AIP Publishing

Experimental and theoretical study of the photodissociation of bromo-3-fluorobenzene

Daniel Karlsson
Department of Photochemistry and Molecular Science, Uppsala University, Box 523, SE-75120 Uppsala, Sweden

O. Anders Borg and Sten Lunell
Department of Quantum Chemistry, Uppsala University, Box 518, SE-75120 Uppsala, Sweden

Jan Davidsson
Department of Photochemistry and Molecular Science, Uppsala University, Box 523, SE-75120 Uppsala, Sweden

Hans O. Karlsson[a)]
Department of Quantum Chemistry, Uppsala University, Box 518, SE-75120 Uppsala, Sweden

(Received 5 October 2007; accepted 6 November 2007; published online 17 January 2008)

The UV photodissociation of bromo-3-fluorobenzene under collisionless conditions has been studied as a function of the excitation wavelength between 255 and 265 nm. The experiments were performed using ultrafast pump-probe laser spectroscopy. To aid in the interpretation of the results, it was necessary to extend the theoretical framework substantially compared to previous studies, to also include quantum dynamical simulations employing a two-dimensional nuclear Hamiltonian. The nonadiabatic potential energy surfaces (PES) were parameterized against high-level MS-CASTP2 quantum chemical calculations, using both the C–Br distance and the out-of-plane bending of the bromine as nuclear parameters. We show that the wavelength dependence of the photodissociation via the $S_0 \rightarrow {}^1\pi\pi^* \rightarrow {}^1\pi\sigma^*$ channel, accessible with a ~260 nm pulse, is captured in this model. We thereby present the first correlation between experiments and theory within the quantitative regime. © *2008 American Institute of Physics*. [DOI: 10.1063/1.2819093]

I. INTRODUCTION

Research on fundamental dynamics of photochemical processes in molecules is an important issue in modern physical chemistry. To actively intervene with and ultimately control the outcome of a light-induced chemical reaction will require detailed knowledge of the critical parameters. The photoreactions of halogen containing diatomics have been extensively-investigated with great success.[1–4] The focus has now turned to accurate studies of larger molecules, such as halogenated methanes,[5–7] and the pioneering work on halogenated aromatic hydrocarbons has been made by Bersohn and co-workers.[8–10] Of course, the studies of larger systems are inherently more difficult, and clear-cut understanding of the, often ultrafast, photochemical processes requires a coupling between time-resolved experiments and theoretical predictions from accurate calculations on excited states.

Ultrafast laser techniques have made experimental determination of subpicosecond photochemical time constants possible,[11,12] and this is now a days routinely made for several types of light-induced processes in many laboratories. On the theoretical side, the accuracy-to-cost ratio for this kind of problems was improved with the introduction of new, computationally cheap, correlated quantum chemical methods such as multiconfigurational perturbation theory.[13–17] However, with the use of quantum chemical *ab initio* methods to model photochemical processes, the number of nuclear degrees of freedom soon becomes a problem. There are essentially two ways of adapting to this, either the molecular model systems needs to be small, such as a diatomic, or allow low-dimensional modeling. When doing this, i.e., including only the most important nuclear degrees of freedom, experiments and theory can be coupled to a low computational cost.

Theoretical quantification can be made by means of quantum dynamics simulations, and validation of the model should be done by comparisons with experiments. This validation has never been done before for halogenated benzenes, and accordingly, experimental kinetic constants have never been shown to be reproduced theoretically. However, halogenated benzenes (X–Ph, X=F, Cl, Br, or I) are suitable model systems, the ring geometry is almost unaffected upon excitation to the lower excited electronic states, and these molecules can be described as two- or three-body problems.

Experimental assessments of the electronic states involved in the UV photodissociation of halobenzenes have been made in the gas phase using photofragment translational spectroscopy by Bersohn and co-workers,[8–10] El-Sayed and co-workers,[18,19] Lou and co-workers,[20–22] and Ichimura *et al.*,[23–27] while more accurate quantifications of the photodissociation processes were made by means of femtosecond time-resolved multiphoton ionization mass spectrometry initially by Cheng *et al.*[28] on iodo benzene and

[a)]Author to whom correspondence should be addressed. Tel.: +46 18 471 32 66. Fax: +46 18 471 58 30. hans.karlsson@kvac.uu.se.

extended to other molecules by Kadi *et al.*,[29–31] Wilkerson and Reilly,[32] and Yuon *et al.*[33] On the basis of these investigations, the mechanism for the major photoinduced carbon-halogen dissociation channel in halogenated benzenes has been assumed to be a spin-orbit mediated transition from the first excited singlet state ($^1\pi\pi^*$) to a low lying repulsive triplet state ($^3n\sigma^*$ or $^3\pi\sigma^*$). The relevance of $^1\pi\sigma^*$ was first assessed in Ref. 34.

The first theoretical throughout assessments, confirming that both $n\sigma^*$ and $\pi\sigma^*$ repulsive electronic states might be of relevance, employed quantum chemical calculations and a model containing one-dimensional potential energy surfaces (PES), with the C–X distance as the geometrical parameter,[35–40] i.e., the simplest possible model for dissociation.

Further, those calculations implied that, not only the repulsive triplet states, but also the singlet correspondences, $^1\pi\sigma^*$ and $^1n\sigma^*$, could be of significance for the dissociation. To model a predissociation reaction quantitatively, the barrier for the transition between the bound and repulsive states must be accurately determined. In the one-dimensional model, the barrier has been approximated by the difference in energy between the crossing points in the C–X direction between the first excited bound singlet and the lowest repulsive state, singlet or triplet, and the photon energy of the laser pulse.[35–40] Problems arose when it was established that this approach was not able to capture more subtle effects such as fluorine substitution of bromobenzene.[40] The one-dimensional model was recently extended with out-of-plane bending of the bromine atom and explicit calculation of spin-orbit effects.[41] In that work, focus was set on finding the lowest accessible transition upon these simple geometrical changes. However, these geometrical alternations resulted in the second lowest electronic state, $n\sigma^*$, and not the lowest, $\pi\sigma^*$. Apart from concluding that the dissociation can be made accessible on a picosecond time scale upon this geometrical alteration, it was also found that the *barrier* for the transition can be captured accurately in a pure singlet calculation.

Even if it is possible to extend the nuclear configurational space and calculate the necessary potential energy surfaces with high accuracy, the question whether the calculation will reproduce the experiments remains. In essence, dynamical properties are addressed and, therefore, a dynamical approach should be chosen also in the theoretical treatment of these problems.

In this work, we isolate the relevant parameters for the photodissociation of a carefully chosen model system, bromo-3-fluorobenzene, using a combination of femtosecond pump-probe laser spectroscopy of molecules in the gas phase, *ab initio* quantum chemical calculations, and quantum dynamics simulations.

The femtosecond pump-probe measurements were performed at different excitation wavelengths to show how the dissociation kinetics depends on the distribution of the population in the excited state. The experimental results are then compared with predicted time constants, obtained by quantum dynamical simulations on PES parameterized against multiconfigurational quantum chemical calculation based upon CASSCF (Ref. 42) and MS-CASPT2.[14–17] We show that it is possible to describe the lowest singlet bound-to-repulsive state transition ($^1\pi\pi \rightarrow \pi\sigma^*$), for a C_S symmetric molecule, with only two internal degrees of freedom, C–Br stretch (d) and C–C–Br out-of-plane bending (α). By choosing a C_s symmetric molecule and comparing with experiments we show, for the first time, that this simple model can be used to quantify the $\pi\pi \rightarrow \pi\sigma^*$ electronic transition. It is also established that this mechanism is the most likely responsible for the depopulation of the first excited singlet state, and in addition, it is possible to exclude several other mechanisms suggested in the literature.

TABLE I. CASSCF optimized ring geometry.

	x (bohr)	y (bohr)	z (bohr)
Hydrogen	2.403	0.000	−3.349
Hydrogen	6.453	0.000	3.705
Hydrogen	2.387	0.000	6.038
Hydrogen	−1.676	0.000	3.716
Carbon	0.128	0.000	0.082
Carbon	0.092	0.000	2.698
Carbon	2.369	0.000	−1.310
Carbon	4.628	0.000	0.085
Carbon	4.666	0.000	2.719
Carbon	2.394	0.000	3.995
Fluorine	6.813	0.000	−1.156

II. DETAILS OF THE QUANTUM CHEMICAL CALCULATIONS

All calculations were done with the MOLCAS 6.2 (Refs. 43 and 44) program package. The two-dimensional PES for the first singlet excited state was calculated at the MS-CASPT2 (Refs. 13–17)/ANO-S (Ref. 45) level with basis set contractions $7s3p/2s1p$ (H) and $10s6p3d/3s2p1d$ (C, F). For bromine, the Barandrian[46] seven-electron ECP basis set $(9s8p4d/1s1p2d)$ was used. The active space contained 12 electrons in ten orbitals. The C_1–Br distance (d) was varied in the range of [1.5 Å, 5.0 Å] and out-of-plane bending angle (α) in the range of [0°, 80°]. The Hamiltonian of the reduced dimensionality model presented above contains only two dimensions, and the ring geometry was therefore frozen. The chosen geometry of the ring was the optimized CASSCF S_0 geometry (Table I). Five vertical adiabatic states were calculated, and from these three diabatic states, S_0, $^1\pi\pi^*$, and $^1\pi\sigma^*$ were parameterized. Details on the adiabatic to diabatic transformation is found in the Appendix.

III. QUANTUM DYNAMICS SIMULATION

The quantum dynamics is modeled as a coupled three state system, reduced to a coupled two state problem when the pump pulse is over. The wave function is represented on a grid with $N_d=240$ and $N_\alpha=256$ grid points, with the action of the kinetic energy operators performed via Fourier transform techniques.[47] The actual wave-packet propagation was performed with the short iterative Lanczos method.[48]

IV. RESULTS AND DISCUSSION

A. Models of the adiabatic potential energy surfaces

From a computational point of view, the spin of the system at the $\pi\pi^*/\pi\sigma^*$ saddle point needs to be known to be able to model the dissociation properly. Large spin-orbit effects at and around this point would affect the barrier significantly. The spin character of the repulsive state is subject to discussion, and in a recently published report on 1-Br-3,5-diFPh,[41] it is suggested that the effects of spin-orbit coupling, which would be necessary for enabling a singlet-to-triplet transition, are insignificant up to until the C_1–Br bond is actually broken. After this point, the repulsive state is a 50%-50% mixture of singlet and triplet, i.e., the triplet character becomes significant only *after* the system has passed over a pure singlet barrier. The actual coupling between the bound and repulsive surfaces is mediated by geometrical distortions, while spin-orbit coupling will mix the singlet and triplet repulsive states. This has the practical implication that the spin can be chosen to be singlet, without any significant loss of accuracy in the barrier height. Further, two mechanisms are conceivable, $\pi\pi^* \rightarrow n\sigma^*$ and $\pi\pi^* \rightarrow \pi\sigma^*$. However, the effects of spin-orbit coupling are similar in the two processes, since the bond needs to be broken for the spin-orbit effects to become significant.

The crudest model for disconnecting Br from BrPh uses only the stretch of the C–Br bond as a geometrical parameter in the PES. However, to couple the $^1\pi\pi^*$ state to the $^1\pi\sigma^*$ state, the symmetry induced orthogonality of these states has to be broken. This will require a full reduction of the symmetry of the molecule from C_{2v} to C_1. Starting with only C–Br elongation, the $^1\pi\pi^*$ (B_2 symmetry[40]) and $^1\pi\sigma^*(B_1)$ (Ref. 40) states will not couple, since this geometrical change retains the C_{2v} symmetry. Hence, more dimensions than C–Br have to be included to model the dissociation. Out-of-plane bending of the dissociating atom used for other molecules[49] will reduce the symmetry to C_s.[41] However, the mirror plane orthogonal to the benzene plane is preserved upon this geometry modification, and, therefore, the $^1\pi\pi^*(B_1)$ and $^1\pi\sigma^*(B_2)$ states in C_{2v} symmetry will transform to, yet uncoupled, $^1\pi\pi^*(A')$ and $^1\pi\sigma^*(A'')$ states in C_s symmetry. Thus, at least three coordinates are required to model the $^1\pi\pi^* \rightarrow {}^1\pi\sigma^*$ transition in BrPh. The $^1\pi\pi^* \rightarrow {}^1n\sigma^*$ transition, on the other hand, corresponds to a $B_2 \rightarrow B_2$ transition and is therefore allowed already in C_{2v} symmetry.

The $^1\pi\pi^* \rightarrow {}^1n\sigma^*$ transition corresponds to a larger barrier than the $^1\pi\pi^* \rightarrow {}^1\pi\sigma^*$ ditto, since the former is a two electron process ($\pi \rightarrow n$, $\pi^* \rightarrow \sigma^*$). In Br-3-FPh the initial ground-state symmetry is lowered to C_s by adding fluorine to C_3. This results in A' symmetry for the bound $^1\pi\pi^*$ state and A'' for the repulsive $^1\pi\sigma^*$ state,[40] i.e., the states are still not coupled as long as the molecule is kept planar. Out-of-plane bending of the bromine, however, is a necessary and sufficient geometrical alteration for reducing the symmetry to C_1, this will enable the lowest excited singlet-singlet transition. The lowest electronic transition that leads to C_1-Br dissociation can therefore be investigated by inclusion of only two nuclear degrees of freedom.

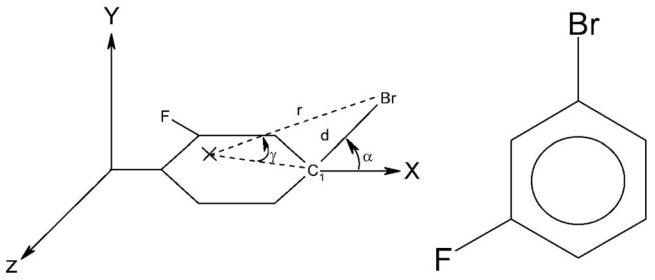

FIG. 1. Br-3-FPh and transformation to three-body system. "X" is the center of mass of the C_5H_4F subsystem.

Screwing of the phenyl ring has earlier been suggested to be of major importance for the dynamics in the S_1 state of chlorobenzene,[34] since it makes $^1\pi\sigma^*$ accessible from $^1\pi\pi^*$. To describe the dynamics in the S_1 state of Br-3-FPh, we have chosen the lowest vibrational eigenmodes, the C–Br stretch and the out-of-plane bending, as internal coordinates. These are associated with the smallest curvature and presumably results in the lowest barriers. The good agreement between simulations and experiment supports our model. On this basis, we conclude that screwing of the phenyl ring is not the most relevant symmetry breaking coordinate.

As in the work by Vallet *et al.*,[49] the two-dimensional model with C_1-Br stretch and out-of-plane bending of the dissociating atom was implemented by transforming the internal d and α coordinates to coordinates for a three-body system (Fig. 1).

B. Experimental results

The Hamiltonian of the simulation contains only intrinsic properties of the molecule, i.e., no effects of the environment are included. To make comparison with experiments more straightforward, the experiments were performed in the gas phase.

The dissociation kinetics was studied in a molecular beam using the pump-probe method, a description of the experimental setup is found in the Appendix. In the experiments, one pump photon (pulse length of 40–65 fs, photon energy: 4.86–4.68 eV) excites the molecules to the $^1\pi\pi^*$ state, and two or more subsequent probe photons (pulse length of ~15 fs, photon energy: 2.30 eV) bring the excited molecules above the ionization limit. Kinetic traces, related to the $^1\pi\pi^*$ lifetime, were obtained by recording the yield of positively charged Br-3-FPh ions, P_E, as a function of the delay between pump and probe pulses.

The kinetic traces were fitted to a biexponential curve,

$$P_E = P_{1E}\exp(-t/\tau_{1E}) + P_{2E}\exp(-t/\tau_{2E}), \quad (1)$$

convoluted with a Gaussian function for the system response,

$$R = R_0\exp(-t/\tau_R)^2. \quad (2)$$

In these equations, τ_{1E} and τ_{2E} represent time constants for the decay, and τ_R is related to the pulse length in the time domain. The best fit parameters for the dissociation process are summarized in Table II. The subpicosecond time constant τ_{1E} does not show any apparent wavelength dependence and, therefore, corresponds to a two-photon excitation of a purely

TABLE II. Best fit parameters for the pump-probe data (index *E*). The corresponding evolution of the population on the S_1 state, obtained from the quantum dynamics simulations (index *S*). The amplitudes P_{ij} have been normalized to unity.

	P_{0s}	P_{1s}	τ_{1s} (ps)	P_{2s}	τ_{2s} (ps)	P_{1E}	τ_{1E} (ps)	P_{2E}	τ_{2E} (ps)
255 nm/4.86 eV	0.08	0.56	1.3	0.36	17.5	0.54 ± 0.08	0.29 ± 0.23	0.46 ± 0.08	5.6 ± 0.9
258 nm/4.81 eV	0.07	0.27	2.3	0.66	26.8	0.46 ± 0.06	0.33 ± 0.10	0.54 ± 0.06	6.2 ± 0.6
260 nm/4.77 eV	0.23	0.13	2.5	0.63	25.2	0.52 ± 0.08	0.71 ± 0.39	0.48 ± 0.08	8.1 ± 0.5
265 nm/4.68 eV	0.77	⋯	⋯	0.23	66.7	0.47 ± 0.09	0.82 ± 0.24	0.53 ± 0.09	16 ± 2.1

repulsive state, most likely the S_3-A'' ($^1\pi\sigma^*$) state with a vertical excitation energy of 8.29 eV,[40] and is therefore not relevant for the dynamics of the $^1\pi\pi^*$ state. The actual lifetime of the $^1\pi\pi^*$ state is described by the wavelength dependent time constant $\tau_{2E} \sim 5.6-16$ ps. If the ultimate goal is to control the outcome of chemical reactions, it is a complication to have two different states initially populated, this might be avoided by exciting with pulses of lower intensity.

In a previous paper,[40] we reported two time constants, 15.6 and 44.1 ps, for Br-3-FPh when pumping with longer pulses at 270 nm ($\tau_{\mathrm{FWHM}} \sim 120$ fs). The first time constant of 15.6 ps was ascribed to excitation of a triplet state with a low barrier for dissociation. This channel could not be found in the present study at any wavelength between 255 and 265 nm. The absence of the pure triplet channel at these excitation wavelengths can be understood since the energy of the triplet state is slightly below the S_1 state. Accordingly, the probability of exciting that triplet state at higher excitation energies is low. When increasing the pump wavelength to 270 nm, which corresponds to exciting the red edge of the ^1L_b band, a second picosecond time constant could barely be seen in the present experimental setup as well. This time constant will not be discussed any further in this paper. The second time constant of 44.1 ps from Ref. 40 was identified with the $^1\pi\pi^*$ state lifetime, and is in line with τ_{2E} found in the present study, see Fig. 4.

Interestingly enough, τ_{2E} decreases smoothly with decreasing pump wavelength, from 16 ps at 265 nm to 5.6 ps at 255 nm. That is, increasing the pump energy by no more than 0.12 eV causes almost a threefold decrease in τ_{2E}, this sets large requirements on the accuracy in the simulations to get quantitatively reliable results. Also, the correlation between pump wavelength and excited state lifetime indicates that the same excited state, $^1\pi\pi^*$, is reached at all wavelengths.

C. Results from simulations

The nonadiabatic representation of the PES can be parameterized in several ways.[50] In this work, we have chosen analytical shapes of the PES on the basis of chemical knowledge, and with the requirement that the least square fitted adiabatic PES should be in good agreement with the quantum chemically calculated ditto. The methods used in the quantum dynamical calculations are described in the Appendix. As an independent test of the reliability, we compared the simulated results based on the PES with experimental data. This study therefore provides a test of the accuracy of a methodology based upon chemical understanding. In Fig. 2, the coupling region of the diabatic (nonadiabatic) and adiabatic surfaces is displayed.

The coupling has the form $\Lambda = \tanh(f(d))\sin(g(\alpha))$, and this separates the surfaces at $d = 2.15$ Å, $\alpha \neq 0$. A sinus shape in the α direction when $d < 2.15$ Å on both S_1 and S_2 is seen. It was established that the major factor affecting the kinetics is the magnitude of the coupling, while the shape is not so important. Any population reaching the repulsive S_2 surface disappears on a femtosecond time scale, while the S_1 surface will retain a significant population for some picoseconds. A biexponential function was fitted to the simulated time dependence of the population P_S in the S_1 state,

$$P_S = P_{0S} + A_{1S}\exp\left(-\frac{t}{\tau_{1S}}\right) + A_{2S}\exp\left(-\frac{t}{\tau_{2S}}\right). \tag{3}$$

In this equation, τ_{1S} and τ_{2S} are time constants related to the lifetime of the S_1 state, and P_{0S} is the remaining population at infinite time. The simulated and measured time constants were obtained using similar functions, Eqs. (3) and (1), respectively, and could thereby be compared to evaluate the model, see Table II and Fig. 4.

In the experiment, one or several ring-breathing modes are Franck-Condon (FC) active, i.e., they are ring-breathing modes that are initially excited by the pump pulse. This excess vibrational energy is transferred to the C_1-Br stretch and

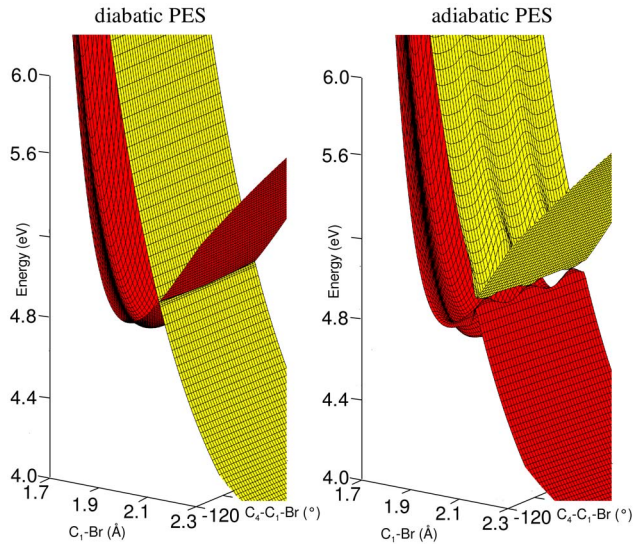

FIG. 2. (Color online) Diabatic (left) and adiabatic (right) potential energy surfaces for the bound- and repulsive-singlet states. The S_1 population evolves initially on the bound (red, left) PES, to be transferred to the repulsive (yellow, left).

C_4-C_1-Br out-of-plane bending modes, henceforth referred to as "reactive" modes. In the simulation, the ring-breathing modes are not included, and, therefore, the process of energy redistribution from the FC-active to the reactive modes is also neglected. In the simulation, the lifetime of the S_1 state will therefore only depend on which vibrational states of the C–Br stretching mode and C–C–Br out-of-plane mode that are populated and their respective lifetimes. The distribution of the population on the α and d modes is determined by the excitation energy, the bandwidth of the excitation pulse, and the FC overlap between the vibronic levels of the S_0 and S_1 states.

It can *a priori* be expected that the population will be distributed between several eigenmodes in the S_1 state. The simulated pump pulse is set to be 50 fs wide in the time domain, $\tilde{\nu}_{\mathrm{FWHM}}$ is 340 cm^{-1} at 260 nm, and both α and d corresponds to low-frequency vibrations, i.e., the energy spacing between the vibrational states on the S_1 surface are small. As many as 72 vibronic levels are found within the first 1160 cm^{-1}. At lower excitation energies, typically 20 vibrational states are significantly populated, with the first vibronic level carrying the major part of the population. The lifetime of the population in a particular vibrational state is determined by the coupling strength between the S_1 and S_2 states, Λ, i.e., Λ determines the reaction barrier. The first vibrational levels have too low energy to overcome the reaction barrier and are essentially bound. Only negligible resonances are present, reflecting the low tunneling probability for heavy atoms such as bromine. The vibrational states at slightly higher energy have lifetimes in the order of 20–30 ps. At energies higher than 4.82 eV, the vibronic levels with lifetimes shorter than 3 ps appear. These three time scales, $\geqslant$100, 20–30, and $<$3 ps, could be captured by the biexponential function, as in Eq. (3), where the population in the essentially bound states is described by the constant factor P_{0S}.

D. Evaluation of the model

In Figs. 3 and 4 and Table II, the results comparing experiments and simulations are collected. The magnitude of the P_{0S} parameter increases rapidly at energies below 4.81 eV which implies that, at lower excitation energies, mostly bound vibrational states are reached. In the experiments, on the other hand, the observed ion signal reaches zero at long pump-probe delay times for all excitation wavelengths between 255 and 270 nm,[40] indicating that no bound states are populated. The absence of bound states is also supported by a very low yield of fluorescence and phosphorescence in a very similar molecule, bromobenzene.[52] One reason for not populating bound vibrational states in the experiments is that the energy of the lowest FC-active mode corresponds to excited vibrational modes of the reactive mode. This prevents the low energy bound vibrational states in the reactive domain to be populated to any large extent.

Provided the model represented by Eq. (3), the kinetics of the S_1 state in the simulations is captured by two time constants, $\tau_{1S} \sim 1.3–2.5$ ps and $\tau_{2S} \sim 17.5–66.8$ ps, which can be directly compared with the experimental time constant, $\tau_{2E} \sim 5.4–16$ ps, at excitation energies between 4.86 and 4.68 eV, see Figs. 3 and 4. Another approach to compare results and simulations, which is not dependent on assumptions about the functional form of the decay kinetics, is by evaluating the root-mean-squared deviation (RMSD) between the simulated and experimentally determined decay

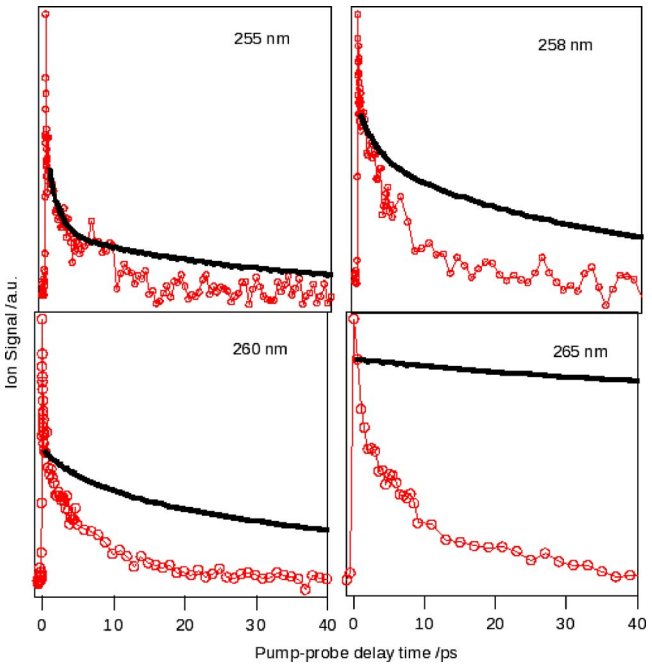

FIG. 3. (Color online) Experimental results (open circles) compared with results from quantum dynamic simulations (thick line). The fast component of the experimental trace is associated with a two-photon excited state that is not included in the simulation. To make a correct comparison with the simulated results, the amplitude was adjusted to that of the experimental trace at roughly 0.5 ps.

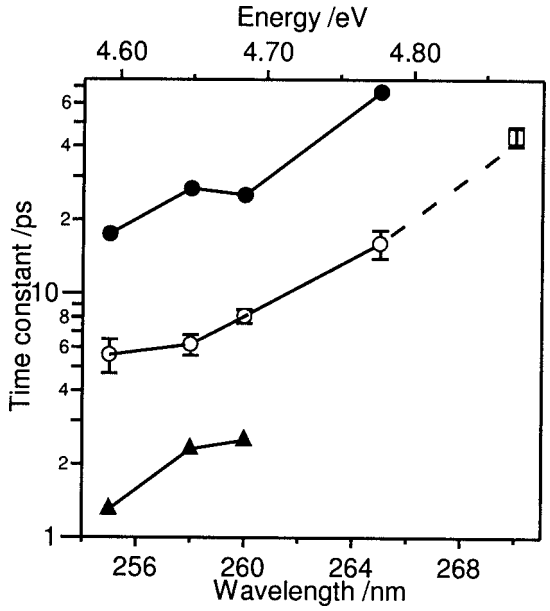

FIG. 4. Time constants for the S_1 lifetime at different energies. Open symbols represent experimental time constants, circles correspond to τ_2 obtained in this study, and the square is data from Ref. 40. Filled symbols represent simulated time constants, and τ_1 and τ_2 correspond to a triangle and a circle, respectively.

curves. This analysis gives RMSD values of 0.158 and 0.634 ps for 4.86 and 4.68 eV, respectively, see Fig. 3. Using either of these evaluation methods, we see that the experimental and simulated results agree well, especially at higher excitation energies. The discrepancy between simulations and experiments is likely an effect of neglecting the coupling between the initially excited, FC-active modes and the reactive modes. Thus, the population of the reactive modes generated in simulation is therefore likely to be somewhat different compared to the experiments.

Despite the employed approximations, we are able to capture the major features of the decay mechanism. The simulated time constants are in good agreement with the measured time constants which indicate that the S_1 lifetime is determined by dissociation of bromine from the phenyl ring via a $^1\pi\pi^* \rightarrow {}^1\pi\sigma^*$ electronic transition, as our model requires.

V. SUMMARY AND CONCLUSIONS

The objective of this work was to find a quantitative model for the depopulation of the first excited bound singlet state in fluorinated bromobenzenes, and in doing so establish which geometrical, multiplicity, and symmetry features are of relevance. Thus, the $^1\pi\pi^* \rightarrow {}^1\pi\sigma$ mechanism was investigated. This is the most important mechanism from an experimental point of view since it is the lowest singlet-singlet transition from a bound to repulsive state. We thereby complete our previous work by carefully examining this pathway and excluding radiative decay, hot-molecule mechanisms, and internal conversion as being of major relevance. For this, we used ultrafast laser spectroscopy and two-dimensional quantum dynamics simulations. The simulations were based on nonadiabatic potential energy surfaces, parameterized towards quantum chemical *ab initio* energies using a unitary transformation, with the C–Br elongation and bromine out-of-plane bending as geometrical parameters. The experimental results show that the S_1 lifetime increases smoothly with increasing excitation energy, from 5.6 ps at 255 nm to 16 ps at 265 nm. Employing the same excitation wavelengths in the simulations as in the experiments, two time constants of ~1.3–2.5 and ~17.5–66.7 ps fit the time evolution of the excited state population. That is, the dissociation characteristics can be described in an almost quantitative regime using the reduced dimensionality model, mainly since the out-of-plane bending reduces the molecular symmetry to C_1 which enables the coupling between the bound $^1\pi\pi^*$ state and the repulsive $^1\pi\sigma^*$ state.

In essence, we find that, to quantify the C–Br photolysis, it is necessary to include at least two dimensions, C–Br stretch and Br out-of-plane bending, and this process can be described using pure singlet states.

ACKNOWLEDGMENTS

The Swedish Research Council (VR) and the Wallenberg Foundation are gratefully acknowledged for financial support. The Uppsala Multidisciplinary Center for Advanced Computational Science (UPPMAX) is acknowledged for grants of computer time.

TABLE III. Parameters of the nonadiabatic PES, the numbers have been truncated.

S_0	S_1	S_2	Unit
$x_{01}=3.309$	$x_{11}=2.000$	$x_{21}=8.909$	eV
$x_{02}=1.738$	$x_{12}=1.966$	$x_{22}=1.470$	$Å^{-1}$
$x_{03}=1.935$	$x_{13}=1.938$	$x_{23}=1.566$	Å
	$x_{14}=4.694$	$x_{24}=3.435$	eV
$A_1=590.2$	$B_1=2.440$	$C_1=2.919$	eV
$A_2=0.129$	$B_2=1.682$	$C_2=1.141$	Å
$A_3=1.341$	$B_3=0.157$	$C_3=0.008$	$Å^{-1}$
$k_{02}=0.298$	$k_{12}=1.029$	$k_{22}=1.070$	rad^{-1}

APPENDIX A: THE ADIABATIC TO DIABATIC TRANSFORMATION

The dynamics of the photoreactions investigated here has some intrinsic complications in regarding the modeling. The way in which chemical structures and reactions are usually modeled, which is also the way in which most quantum chemical software works, is built upon the adiabatic approximation.[51] This approximation has its origin in that the electronic and nuclear degrees of freedom of the molecules are separated: the approximation is justified when the system moves slowly and the energy levels (the electronic energy levels in the adiabatic approximation) are energetically well separated. Neither of these two requirements are fulfilled in the critical region of excited state PES here, i.e., where the electronic structure changes from being bound to repulsive. To build up a correct description of these photoreactions, one therefore has to go beyond the adiabatic approach.

In this work, the procedure for adiabatic to diabatic transformation described thoroughly by, e.g., Domcke and co-workers,[49,51] was used. In this procedure, energy eigenvalues calculated in an adiabatic framework are fitted towards unitarily transformed analytic functions assumed to describe the diabatic PES and the couplings between them. All parameters are in Table III.

First, the S_0 surface was assumed to be uncoupled to any other surface. The $\pi\pi^*(S_1)$ and $\pi\sigma^*(S_2)$ surfaces, on the other hand, are coupled around the $\pi\pi^*/\pi\sigma^*$ crossing if $\alpha > 0°$. To describe the area around the S_1/S_2 intersection, a 2×2 matrix was used,

$$V = \begin{bmatrix} S_1 & \Lambda \\ \Lambda & S_2 \end{bmatrix}. \tag{A1}$$

In this ansatz, S_1 and S_2 are the energies of the diabatic $^1\pi\pi^*$ and $^1\pi\sigma^*$ states for a particular point (d,α), and Λ is the coupling in that point. The parameters of the diabatic PES and the coupling functions were found by fitting the eigenvalues of this matrix by a least-square procedure to the quantum chemically calculated energy eigenvalues.

The functional forms of the PES were chosen as follows. The S_0 surface was assumed to be a Morse potential in the d direction (v_{00}), added to a cosine function in the α direction (v_{01}) whose influence is switched off by ν_{02} as d increases. Explicitly, the chosen function is

$$S_0 = \nu_{00}(d) + \nu_{01}(d)\nu_{02}(\alpha), \tag{A2}$$

with

$$\nu_{00}(d) = x_{01}(1 - \exp(-x_{02}(d - x_{03})))^2, \tag{A3}$$

$$\nu_{01}(\alpha) = 1 - \cos(k_{02}\alpha), \tag{A4}$$

and

$$\nu_{02}(d) = \frac{1}{2}A_1\left(1 - \tanh\left(\frac{d - A_2}{A_3}\right)\right). \tag{A5}$$

The $^1\pi\pi^*(S_1)$ surface can be parameterized with the same functions since the $\pi \rightarrow \pi^*$ excitation is located to the ring and does not really affect d or α. That is,

$$S_1 = \nu_{10}(d) + \nu_{11}(d)\nu_{12}(\alpha) \tag{A6}$$

with

$$\nu_{10}(d) = x_{11}(1 - \exp(-x_{12}(d - x_{13})))^2 + x_{14}, \tag{A7}$$

$$\nu_{11}(d) = \frac{1}{2}B_1\left(1 - \tanh\left(\frac{d - B_2}{B_3}\right)\right), \tag{A8}$$

and

$$\nu_{12}(\alpha) = (1 - \cos(k_{12}\alpha))^2. \tag{A9}$$

The least square fit of this surface started with the $\alpha = 0$ cross section (ν_{10}), followed by ν_{11} and ν_{12} with a larger weight to the area $d < 2.15$ Å, that is, before the S_1/S_2 crossing, so that the region most important for reproducing kinetic constants is properly described. The $^1\pi\sigma^*(S_2)$ surface is described by the same functional form as the other surfaces, but with different parameters, that is,

$$S_2 = \nu_{20}(d) + \nu_{21}(d)\nu_{22}(\alpha), \tag{A10}$$

with

$$\nu_{20}(d) = x_{21}(1 - \exp(-x_{22}(d - x_{23})))^2 + x_{24}, \tag{A11}$$

$$\nu_{21}(r) = \frac{1}{2}C_1\left(1 - \tanh\left(\frac{d - C_2}{C_3}\right)\right), \tag{A12}$$

and

$$\nu_{22}(\alpha) = (1 - \cos(k_{22}\alpha))^2. \tag{A13}$$

Here, the area $d > 2.15$ Å was considered as most important since the wave packet can be assumed to propagate on this part of the surface.

Finally, the coupling was parameterized. It is sinus-square shaped in the α direction and is turned off after 2.15 Å,

$$\Lambda = \lambda_d(d)\lambda_\alpha(\alpha), \tag{A14}$$

where

$$\lambda_d(d) = \lambda_0\left(1 - \tanh\left(\frac{d - \lambda_1}{\lambda_2}\right)\right), \tag{A15}$$

and

$$\lambda_\alpha(\alpha) = (\sin(\lambda_3\alpha))^2. \tag{A16}$$

The following parameters were obtained for the coupling, Eqs. (A14)–(A16); $\lambda_0 = 0.132$ eV, $\lambda_1 = 2.160$ Å, $\lambda_2 = 0.011$ Å^{-1}, and $\lambda_3 = 2.002$ rad^{-1}. Note that these parameters are truncated.

APPENDIX B: THE EXPERIMENTAL SETUP

The experimental arrangement consisted of a femtosecond laser system, a pump-probe setup, a molecular beam source, and a linear time-of-flight (TOF) mass selector. In this setup, the output from a 1 kHz femtosecond laser (Vitesse 800, Coherent Inc.) was amplified with a amplifying system consisting of a Ti:sapphire amplifier (Legend-F, Coherent, Inc.) pumped by a *Q*-switched diode-pumped laser (Evolution, Coherent, Inc.). The output pulses (800 nm, 2.5 mJ, <100 fs) were split in four fractions using beam splitters, of which two fractions were not used. The other two fractions constituted the pump and probe and were subsequently led into separate optical parametric amplifiers (TOPAS-white, Light Conversion). The TOPASes generated a tunable output in the visible range between 500 and 750 nm.

The UV pump pulse (255–265 nm, $\lambda_{\mathrm{FWHM}} \sim 2.3$–$3.0$ nm, $\tau_{\mathrm{FWHM}} \sim 40$–$65$ fs) was generated by frequency doubling the output from the TOPAS using a second harmonic generator (Light Conversion). The probe pulse ($\lambda \sim 540$ nm, $\lambda_{\mathrm{FWHM}} \sim 22$ nm, $\tau_{\mathrm{FWHM}} \sim 15$ fs) was delayed with respect to the pump pulse using a retro reflector mounted on a translational stage (PI, C-842). Variable attenuators were placed in the pump and probe beams to adjust the energy before entering the molecular beam. The polarization of the laser beams were kept at magic angle by adjusting the polarization of the pump beam using a Berek compensator.

The effusive beam of 3-BrFPh was produced in a two chamber oven with an exit aperture of 0.1 mm. The chamber and exit aperture was kept at room temperature. The molecular beam was passed into a Wiley-McLaren TOF setup in the second vacuum chamber. The laser beams were overlapped with the molecular beam in the ionization region of the TOF using a focusing mirror. The formed photoions traversed a flight distance of about 0.3 m before entering the detector, which consisted of a dynode-scintillator-photomultiplier arrangement.

An oscilloscope (Tektronix, TDS 5052B) was used to record the yield of ions in a 20 μs TOF window usually set between 10 and 30 μs with a resolution of 0.08 μs, detecting all positively charged fragments with masses between 10 and 245 u. An average of 1000 laser shots was recorded at each pump-probe delay (time point). Each time scan consisted of 80–160 time points, and one measurement consisted of an average of typically 5–10 time scans.

A small background signal due to multiphoton ionization from the ground state was detected. This signal is convenient to use for finding the best spatial overlap between the pump and the probe. It was proportional to the laser intensity and the amount of molecules in the beam and was also used for normalization purposes. In the time-resolved experiments, low laser intensities were used in order to minimize contribution from this back ground signal.

The main peak in the TOF spectrum corresponded to 3-$BrFC_6H_4^+$, it was selected to determine the kinetics of the excited molecules. The kinetics was found to be similar regardless of which ionic species was used in the measurements.

[1] J. G. Dojahn, E. C. M. Chen, and W. E. Wentworth, J. Phys. Chem. **100**, 9649 (1996).
[2] J. H. Baxendale, J. Phys. Chem. **95**, 8028 (1991).
[3] P. K. Walhout, J. Phys. Chem. **99**, 7568 (1995).
[4] J. M. Papanikolas, Int. J. Radiat. Phys. Chem. **7**, 587 (1975).
[5] Y. Wada, M. Taira, D. Y. Zheng, and S. Yanagida, New J. Chem. **18**, 589 (1994).
[6] D. Ajita, M. Wierzbowska, R. Lindh, and P. Å. Malmqvist, J. Chem. Phys. **121**, 5761 (2004).
[7] Y. J. Liu, D. Ajitha, J. Wisborgh-Krogh, A. N. Tarnovsky, and R. Lindh, ChemPhysChem **7**, 955 (2006).
[8] M. Dzvonik, S. Yang, and R. Bersohn, J. Chem. Phys. **61**, 4408 (1974).
[9] M. Kawasaki, S. J. Lee, and R. Bersohn, J. Chem. Phys. **66**, 2647 (1977).
[10] A. Freedman, S. C. Yang, M. Kawasaki, and R. Bersohn, J. Chem. Phys. **72**, 1028 (1980).
[11] A. H. Zewail, J. Phys. Chem. **97**, 12427 (1993).
[12] A. H. Zewail, J. Phys. Chem. A **104**, 5660 (2000).
[13] K. Andersson, P. Å. Malmqvist, B. O. Roos, A. J. Sadlej, and K. Wolinski, J. Phys. Chem. **94**, 5483 (1990).
[14] K. Andersson, P. Å. Malmqvist, and B. O. Roos, J. Chem. Phys. **96**, 1218 (1992).
[15] J. Finley, P. Å. Malmqvist, B. O. Roos, and L. Serrano-Andres, Chem. Phys. Lett. **288**, 299 (1998).
[16] P. Å. Malmqvist and B. O. Roos, Chem. Phys. Lett. **155**, 189 (1989).
[17] P. Å. Malmqvist, B. O. Roos, and B. Schimmelpfennig, Chem. Phys. Lett. **357**, 230 (2002).
[18] J. E. Freitas, H. J. Hwang, and M. A. El-Sayed, J. Phys. Chem. **97**, 12481 (1993).
[19] H. J. Hwang and M. A. El-Sayed, J. Chem. Phys. **96**, 856 (1992).
[20] H. Zhang, R.-S. Zhu, G.-J. Wang, K.-L. Han, G.-Z. He, and N.-Q. Lou, J. Chem. Phys. **110**, 2922 (1999).
[21] X.-B. Gu, G.-J. Wang, J.-H. Huang, K.-L. Han, G.-Z. He, and N.-Q. Lou, J. Phys. Chem. A **105**, 354 (2001).
[22] R.-S. Zhu, H. Zhang, G.-J. Wang, X.-B. Gu, K.-L. Han, G.-Z. He, and N.-Q. Lou, Chem. Phys. Lett. **300**, 483 (1999).
[23] T. Ichimura, Y. Mori, H. Shinohara, and N. Nishi, Chem. Phys. Lett. **122**, 51 (1985).
[24] T. Ichimura, Y. Mori, H. Shinohara, and N. Nishi, Chem. Phys. Lett. **122**, 55 (1985).
[25] T. Ichimura, Y. Mori, H. Shinohara, and N. Nishi, Chem. Phys. Lett. **125**, 263 (1986).
[26] T. Ichimura, Y. Mori, H. Shinohara, and N. Nishi, Chem. Phys. Lett. **189**, 117 (1994).
[27] T. Ichimura, Y. Mori, H. Shinohara, and N. Nishi, J. Chem. Phys. **107**, 835 (1997).
[28] P. Y. Cheng, D. Zhong, and A. H. Zewail, Chem. Phys. Lett. **237**, 399 (1995).
[29] M. Kadi, J. Davidsson, A. N. Tarnovsky, M. Rasmusson, and E. Åkesson, Chem. Phys. Lett. **350**, 93 (2001).
[30] M. Kadi and J. Davidsson, Chem. Phys. Lett. **378**, 172 (2003).
[31] M. Kadi, E. Ivarsson, and J. Davidsson, Chem. Phys. Lett. **384**, 35 (2004).
[32] C. W. Wilkerson, Jr. and J. P. Reilly, Anal. Chem. **62**, 1804 (1990).
[33] L. Yuan, Y. Wang, L. Wang, J. Bai, and G. He, Sci. China, Ser. B: Chem. **47**, 283 (2004).
[34] A. L. Sobolewski and W. Domcke, Chem. Phys. **259**, 181 (2000).
[35] M. Rasmusson, R. Lindh, N. Lascoux, A. N. Tarnovsky, M. Kadi, O. Kuhn, V. Sundström, and E. Åkesson, Chem. Phys. Lett. **367**, 759 (2002).
[36] Y.-J. Liu, P. Persson, and S. Lunell, J. Phys. Chem. A **108**, 2339 (2004).
[37] Y.-J. Liu, P. Persson, and S. Lunell, J. Chem. Phys. **121**, 11000 (2004).
[38] Y.-J. Liu, P. Persson, H. O. Karlsson, S. Lunell, M. Kadi, D. Karlsson, and J. Davidsson, J. Chem. Phys. **120**, 6502 (2004).
[39] Y. J. Liu and S. Lunell, Phys. Chem. Chem. Phys. **7**, 3938 (2005).
[40] O. A. Borg, Y. J. Liu, P. Persson, S. Lunell, D. Karlsson, M. Kadi, and J. Davidsson, J. Phys. Chem. A **110**, 7045 (2006).
[41] O. A. Borg, Chem. Phys. Lett. **436**, 57 (2007).
[42] B. O. Roos, P. R. Taylor, and P. E. M. Siegbahn, Chem. Phys. **48**, 157 (1980).
[43] G. Karlström, R. Lindh, P. Å. Malmqvist, B. O. Roos, U. Ryde, V. Veryazov, P. O. Widmark, M. Cossi, B. Schimmelpfennig, P. Neogrady, and L. Seijo, Comput. Mater. Sci. **28**, 222 (2003).
[44] V. Veryazov, P. O. Widmark, L. Serrano-Andres, R. Lindh, and B. O. Roos, Int. J. Quantum Chem. **100**, 626 (2004).
[45] K. Pierloot, B. Dumez, P. O. Widmark, and B. O. Roos, Theor. Chim. Acta **90**, 87 (1995).
[46] Z. Barandiaran and L. Seijo, Can. J. Chem. **70**, 409 (1992).
[47] M. D. Feit, J. A. Fleck, Jr., and A. Steiger, J. Comput. Phys. **47**, 412 (1982).
[48] T. J. Park and J. C. Light, J. Chem. Phys. **85**, 5870 (1986).
[49] V. Vallet, Z. Lan, S. Mahapatra, A. L. Sobolewski, and W. Domcke, J. Chem. Phys. **123**, 144307 (2005).
[50] W. A. Jasper, S. Nangia, C. Zhu, and D. G. Truhlar, Acc. Chem. Res. **39**, 101 (2006).
[51] *Conical Intersections: Electronic Structure, Dynamics and Spectroscopy*, edited by W. Domcke, D. R. Yarkony, and H. Köppel (World Scientific, Singapore, 2004).
[52] E. H. Gilmore, G. E. Gibson, and D. S. McClure, J. Chem. Phys. **20**, 829 (1952).